

Trajectory Optimization in Maximal Coordinates

Brian E. Jackson*
Robotics Institute
Carnegie Mellon University
Pittsburgh, USA
brianjackson@cmu.edu

Abstract—A cool abstract

I. MOTIVATION

In order for autonomous robotic systems to operate successfully and robustly in the real world, they need to be able to generate and execute motion plans. Ideally, these motion plans should be able to balance competing objectives such as time-to-arrival, energy efficiency, or safety, handle a broad range of complex scenarios, and be fast to compute so that new plans may be quickly regenerated as the environment around the robot changes. For robotic systems with few degrees of freedom, such as autonomous cars, quadrotors, planes, or underwater robots, the task of efficiently generating and following motion plans, at least for moderately complex scenarios, is relatively straightforward. Approaches to the motion planning problem for these systems include sampling-based methods that sample over the configuration space of the robot and connect samples based on their feasibility [1], graph-based methods that discretize the planning space, and optimization-based methods [2]–[5] that discretize and optimize a single planned trajectory.

While many autonomous systems of interest fall into the previously-mentioned category, many do not. Multi-body systems such as quadrupeds, humanoids, or robotic manipulators can easily have between 20-100 degrees of freedom. Moving into distributed or multi-agent systems such as power or communication networks, multi-agent teams [6], satellite constellations, or swarms of micro-robots, the dimensionality grows to hundreds of degrees of freedom. And for other systems, such as soft robotics or fluid control where the fidelity of the system dynamics is dependent on discretizing a continuous system into a set of finite elements, the number of degrees of freedom becomes arbitrarily large. While the dimensionality of the state vectors describing these systems is often very large, they almost have a unique and sparse coupling between elements of the state: e.g. links in a robot arm are only connected to 1-3 other, links via joints, members of a multi-agent team often only communicate locally with the robots with a given radius, or finite elements that only couple directly with their neighboring elements. When these systems are linearized about some point, this structure shows up as sparsity in the underlying matrices, where often 80-99% of the matrix is zeros, and only 1-20% contains meaningful data. Leveraging this inherent sparsity in the system dynamics is naturally critical to generating efficient motion plans for these systems.

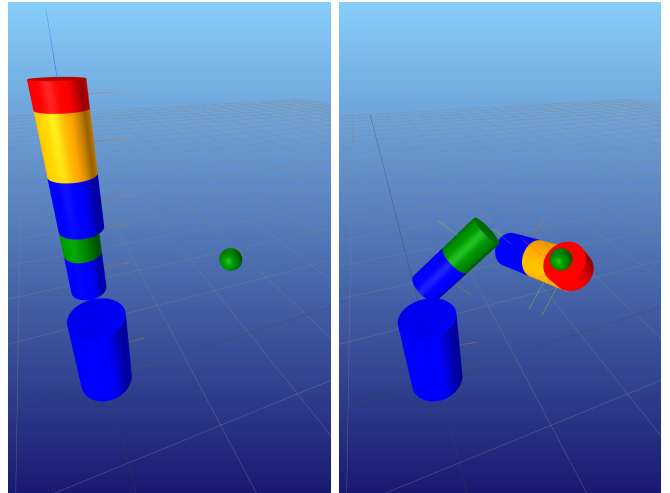


Fig. 1: Arm task of moving from an upright position to a goal location specified in cartesian coordinates. The state and control trajectory was found by solving a trajectory optimization problem in maximal coordinates using Ipopt.

While sampling-based and graph-based methods for motion planning work well for systems of few dimensions, they become computationally intractable above a dozen or so dimensions, thanks to the infamous “curse of dimensionality.” Optimization-based approaches, on the other hand, do not suffer from the same poor scaling properties, and large-scale optimization with millions of decision variables is relatively common in the areas of operations research and machine learning. Unlike many of the problems in these areas, which are either formed as well-structured unconstrained nonlinear optimization, problems Linear Programs (LPs), or Quadratic Programs (QPs)—all of which have mature and sophisticated algorithms and software implementations for efficiently solving large optimization problems—optimization-based motion planning problems such as trajectory optimization are nonlinear programs (NLPs) with nonlinear equality constraints that often make the problem extremely difficult to solve. Only a few general-purpose off-the-shelf NLP solvers are commonly used or under active development [7], [8].

The purpose of this project is to demonstrate the performance of the well-known Ipopt solver when solving motion planning problems for systems with lots of sparsity in the dynamics. In particular, this project focuses on implementing trajectory optimization in maximal coordinates using discrete

variational integrators. Representing rigid-body systems in maximal coordinates has some appealing properties, namely that world or task-based goals and constraints, such as the location of an end-effector for manipulation tasks, are trivially expressed in maximal coordinates. Additionally, some recent studies have shown that local control methods such as LQR perform better in maximal coordinates, which is understandable given that the local linearization of a system in maximal coordinates provides more information than one expressed in minimal coordinates [9], [10]. Lastly, by treating a mechanism as a finite set of individual rigid bodies linked together by joints, we can achieve an extremely high degree of generality and potentially open the door for parallelizable algorithms that will hopefully more than offset the cost of solving a larger optimization problem [11]. While some researchers have attempted this approach in the past with disappointing results [12], this project leverages state-of-the-art variational integrators which offer many benefits over the more traditional integration methods used in previous studies [9], [13], [14]. No previous paper has published any successful results using this approach, so the goal of this paper is to explore the potential of this approach.

II. BACKGROUND

A. Rigid Bodies

A rigid body is a mathematical abstraction that is often extremely useful for describing physical systems whose internal dynamics (such as bending modes) are much higher than the dynamics of interest. Examples include the structurally stiff links used in classical robot manipulators. Many robotic systems are well-approximated by a set of rigid bodies held together by joints. For this paper we will deal exclusively with this type of system, and this section presents the notation and some key equations that arise when dealing with rigid bodies.

1) *Rigid Body State*: The state of a rigid body is typically defined by its three-dimensional pose $x \in SE(3)$ and its velocity $v \in TSE(3) \equiv \mathbb{R}^6$. For convenience, we will often split the pose and velocity into their translational and rotational components:

$$x = \begin{bmatrix} r \\ q \end{bmatrix}, \quad v = \begin{bmatrix} \nu \\ \omega \end{bmatrix} \quad (1)$$

where $r \in \mathbb{R}^3$ is the position of the body in the world frame, $q \in SE(3)$ is the attitude of the body, mapping vectors in the body frame to the world frame, $\nu \in \mathbb{R}^3$ is the linear velocity, and $\omega \in \mathbb{R}^3$ is the angular velocity.

2) *Attitude Representation*: This project represents the attitude as a quaternion in Hamilton form:

$$q = \begin{bmatrix} q_s \\ q_v \end{bmatrix} \quad (2)$$

where $q_s \in \mathbb{R}$ and $q_v \in \mathbb{R}^3$ are the scalar and vector part of the quaternion. Although the space of unit quaternions technically represents a double-cover of the space of rotations, and our state vector is therefore an element of $\mathbb{R}^3 \times \mathbb{S}^3$, we will still denote our state vector as element of $SE(3)$ for brevity.

Using the same notation from [15], we define quaternion multiplication as

$$q_2 \otimes q_1 = L(q_2)q_1 = R(q_1)q_2 \quad (3)$$

where $L(q)$ and $R(q)$ are orthonormal matrices defined as:

$$L(q) = \begin{bmatrix} q_s & -q_v^T \\ q_v & q_s I + [q_v]^\times \end{bmatrix} \quad (4)$$

$$R(q) = \begin{bmatrix} q_s & -q_v^T \\ q_v & q_s I - [q_v]^\times \end{bmatrix} \quad (5)$$

and $[x]^\times$ is the skew-symmetric matrix operator

$$[x]^\times = \begin{bmatrix} 0 & -x_3 & x_2 \\ x_3 & 0 & -x_1 \\ -x_2 & x_1 & 0 \end{bmatrix} \quad (6)$$

We also define the following matrices for convenience:

$$T = \begin{bmatrix} 1 & \\ & -I_3 \end{bmatrix}, \quad (7)$$

$$H = \begin{bmatrix} 0 \\ I_3 \end{bmatrix}. \quad (8)$$

We denote the rotation matrix defined by a unit quaternion as

$$A(q) = H^T L(q) R(q)^T H. \quad (9)$$

3) *Error Pose and Derivatives*: Since our pose is represented with a unit quaternion, we need to account for the unit norm constraint when doing common operations like composing states or taking derivatives. We will frequently need to deal directly with local perturbations about a nominal pose, which we denote by the 6-dimensional error pose:

$$\Delta = \begin{bmatrix} \Delta r \\ \Delta \phi \end{bmatrix} \in \mathbb{R}^6 \quad (10)$$

We can convert from an error pose to a normal pose via an exponential map:

$$\exp(\Delta) = \begin{bmatrix} \Delta r \\ \varphi(\Delta \phi) \end{bmatrix} \in SE(3) \quad (11)$$

where $\varphi(\Delta \phi)$ can be any mapping from a local 3-parameter attitude representation to a unit quaternion¹. For this project, we will use a scaled Cayley map:

$$q = \varphi(\phi) = \frac{1}{\sqrt{1 + \|\frac{1}{2}\phi\|^2}} \begin{bmatrix} 1 \\ \frac{1}{2}\phi \end{bmatrix} \quad (12)$$

The scaling is chosen such that the local perturbations have units on the same scale as radians. The standard exponential map could also be used, but the Cayley map is more computationally efficient.

Composing two poses is done by adding their translations and multiplying their respective quaternions:

$$r_1 \oplus r_2 = \begin{bmatrix} r_1 + r_2 \\ q_1 \otimes q_2 \end{bmatrix} \quad (13)$$

¹As with the scaled Cayley map used here, some care must be taken to ensure the local perturbations are on the scale of radians

When taking derivatives of functions of poses, we expect the derivatives to be with respect to the error pose Δ . Taking the same approach as [15], we get the correct result by differentiating with respect to an error pose composed with the nominal pose, evaluated with an error pose at the additive identity (i.e. zero):

$$\nabla f(x) = \frac{\partial f}{\partial x} \frac{\partial}{\partial \Delta} (x \oplus \exp(\Delta)) \Big|_{\Delta=0} \quad (14)$$

$$= \frac{\partial f}{\partial x} G(x) = \frac{\partial f}{\partial x} \begin{bmatrix} I_3 & \\ & \frac{1}{2} L(q) H \end{bmatrix} \quad (15)$$

where we define $G(x)$ to be the *error pose Jacobian*.

We will also need to differentiate the above equation to obtain second-order derivatives. When doing so, we need to evaluate the derivative of $G(x)^T b$ for some vector $b \in \mathbb{R}^4$ (usually $\partial f / \partial x$). We denote and define this derivative to be:

$$\nabla G(x, b) = \begin{bmatrix} \mathbf{0}_3 & \\ & \frac{1}{2} H^T R(b) T \end{bmatrix} \quad (16)$$

B. Trajectory Optimization

Trajectory optimization is a powerful technique for generating motion plans for complex autonomous systems. Trajectory optimization generally tries to solve problems of the form:

$$\begin{aligned} & \underset{x(t), u(t)}{\text{minimize}} && \ell(x(T)) + \int_0^T \ell(x(t), u(t)) dt \\ & \text{subject to} && \dot{x}(t) = f(x(t), u(t)), \\ & && c_E(x(t), u(t)) = 0, \\ & && c_I(x(t), u(t)) \leq 0, \\ & && x(0) = x_0 \end{aligned} \quad (17)$$

To compute the solution of these infinite-dimensional optimization problems, we generally discretize the trajectories into a set of discrete “knot points”, and approximate the dynamics using some discrete approximation:

$$\begin{aligned} & \underset{x_{1:N}, u_{1:N}}{\text{minimize}} && \ell(x_N) + \sum_{k=1}^{N-1} \ell(x_k, u_k) \\ & \text{subject to} && f_d(x_{k+1}, x_k, u_k), \quad \forall k \in \mathbb{N}_{N-1} \\ & && c_E(x_k, u_k) = 0, \quad \forall k \in \mathbb{N}_N, \\ & && c_I(x_k, u_k) \leq 0, \quad \forall k \in \mathbb{N}_N, \\ & && x_1 = x_0 \end{aligned} \quad (18)$$

where $x \in \mathbb{R}^n, u \in \mathbb{R}^m$ are the state and control vectors, f_d is some discrete approximation of the continuous dynamics, and N is the number of knot points. We define $\mathbb{N}_i = 1, \dots, i$ and $\mathbb{N}_{i,j} = i, \dots, j$.

There are many approaches to solving problems of the form (18). Differential- dynamic programming (DDP) [16], [17] and its variant iterative LQR (iLQR) [4], [18], [19] are some of the most commonly-used methods due to their computational efficiency and relatively straightforward implementation. These methods rely on constructing a local quadratic approximation of the optimal cost-to-go function, which in general is always

dense in the state dimension. This implies that DDP-based algorithms are poorly-suited to leverage structure (i.e. sparsity) in the system dynamics.

The other commonly-used method is direct collocation, which traditionally uses Hermite-Simpson interpolation to “transcribe” the continuous-time problem (17) into a discrete problem of form (18). These generally rely on general-purpose NLP solvers like Ipopt [7], SNOPT [8], or Knitro. Since these solvers all allow the user to provide the sparsity structure of the constraint Jacobians, they can efficiently leverage sparsity in the dynamics. This project uses direct collocation [5], but instead of using the traditional Hermite-Simpson integration, we use a 2nd-order variational integrator, described in the following section.

C. Variational Integrators

The dynamics for many robotic systems can be described using the *manipulator equation*:

$$M(\theta)\ddot{\theta} + C(\theta, \dot{\theta}) + G(\theta) = B(\theta)\tau \quad (19)$$

where $\theta \in \mathbb{R}^n$ are generalized coordinates (often joint angles), $M(\theta)$ is the mass matrix, $C(\theta, \dot{\theta})$ are the Coriolis forces, $G(\theta)$ are the gravitation or potential forces, and $B(\theta)$ maps the torques τ to joint torques. These dynamics can be discretized by solving for $\ddot{\theta}$ and subsequently using any standard quadrature rule, such as a 3rd-order Hermite spline or a 4th-order Runge Kutta method.

The manipulator equation is the result of applying the famous Euler-Lagrange equation to a system of rigid bodies:

$$\frac{d}{dt} \left(\frac{\partial L}{\partial \dot{x}} \right) - \frac{\partial L}{\partial x} = F(t), \quad (20)$$

which itself is just the first-order necessary conditions of the minimum-action principle:

$$\begin{aligned} & \underset{x(t), v(t)}{\text{minimize}} && \int_0^T L(x(t), v(t)) + F(t)^T x(t) \\ & \text{subject to} && \dot{x}(t) = g(v(t)), \\ & && c(x(t)) = 0 \end{aligned} \quad (21)$$

where $L(x, v) = T(x, v) - U(x)$ is the Lagrangian, and $K(x, v), U(x)$ are the kinetic and potential energy of the system. Rather than approximating the discrete dynamics by solving (21) to get the Euler-Lagrange equation, which is then approximated using some integration method, we can instead discretize (21) directly to arrive at a discrete version of the Euler-Lagrange equation. This is the central idea behind discrete mechanics and variational integrators. In the following section we step through the derivation for a 2nd-order variational integrator for systems of rigid bodies.

III. DISCRETE DYNAMICS IN MAXIMAL COORDINATES

Assume we have a system of M rigid bodies, each with state $x^{(j)} \in SE(3)$ and velocity $v^{(j)} \in \mathbb{R}^6$. The concatenated pose and velocity vectors are denoted in bold face: $\mathbf{x} \in M \times SE(3), \mathbf{v} \in \mathbb{R}^{6 \times M}$. Subscript indices are used to denote time steps.

A. Joint Constraints

Let the joints of our multi-body system be defined by a directed graph with nodes $1, \dots, M$, and an edge from i to j denotes a joint between body i and body j . The direction of the edge provides the convention for applying forces and torques on each body. We assume that there is only ever a single edge between a pair of nodes. We denote the graph \mathcal{G} with edge set \mathcal{E} . The function $\mathcal{N}_1(j)$ returns the outbound set of vertices from node j $\{i \mid (j, i) \in \mathcal{E}\}$, and $\mathcal{N}_2(j)$ likewise returns the inbound set of vertices $\{i \mid (i, j) \in \mathcal{E}\}$. The joint constraint function $c(\mathbf{x})$ is then the concatenation of the pairwise joint constraints for each edge in \mathcal{E} . For this project, we will work only with revolute joints, whose pairwise constraint function is:

$$c(x^{(1)}, x^{(2)}) = \begin{bmatrix} r^{(1)} + A(q^{(1)})p_1 - r^{(2)} - A(q^{(2)})p_2 \\ \bar{a}^\perp H^T L(q^{(1)})^T q^{(2)} \end{bmatrix} \quad (22)$$

where p_1 is the location of the joint the link 1 frame, p_2 is the location of the joint in the link 2 frame, \bar{a} is the axis of rotation as a unit vector in the link 1 frame and $\bar{a}^\perp \in \mathbb{R}^{2 \times 3}$ is the orthogonal compliment to the joint axis. This is best computed by taking two consecutive cross products with the joint axis.

B. Joint Forces

Using the same graph as above, we can write functions that provide the forces and torques applied to each body by actuating a joint with a torque $u \in \mathbb{R}$ (for revolute joints). For each pair of indices in the edge set \mathcal{E} (i.e. each joint) we have two functions:

$$\xi_1(x^{(1)}, x^{(2)}, u) = \begin{bmatrix} \mathbf{0}_{3 \times 1} \\ -\bar{a} \cdot u \end{bmatrix} \quad (23a)$$

$$\xi_2(x^{(1)}, x^{(2)}, u) = \begin{bmatrix} \mathbf{0}_{3 \times 1} \\ A(L(q^{(2)})^T q^{(1)}) \bar{a} \cdot u \end{bmatrix} \quad (23b)$$

that return the wrenches on link 1 and 2, respectively. The wrench force is defined in the world frame and the wrench torque is defined in the body frame of each link. The total wrench on any link j is then given by the following expression:

$$\sum_{i \in \mathcal{N}_1(j)} \xi_1(x^{(j)}, x^{(i)}, u_j) + \sum_{i \in \mathcal{N}_2(j)} \xi_2(x^{(i)}, x^{(j)}, u_j) \quad (24)$$

C. Discrete Dynamics

The total kinetic energy of the system is

$$T(\mathbf{x}, \mathbf{v}) = \sum_{j=1}^M \frac{1}{2} (v^{(j)})^T M^{(j)} v^{(j)} \quad (25)$$

and the potential energy, under gravity, is:

$$U(\mathbf{x}) = \sum_{j=1}^M \frac{1}{2} m^{(j)} g r_z^{(j)} \quad (26)$$

Since the pose of our system lies on a manifold, we must enforce the constraint in (18) specifying the state kinematics. We wish to approximate the midpoint velocity using two

consecutive poses separated by a time step of h seconds. For linear velocity, this is just $\frac{1}{2}(r_2 - r_1)$. For angular velocity, we use the quaternion kinematics:

$$\dot{q} = \frac{1}{2} L(q) H \omega. \quad (27)$$

We can approximate the quaternion at the next time step using Euler integration and re-arranging to isolate q_1 , where we use q_I to represent the quaternion identity:

$$q_2 \approx q_1 + h \dot{q}. \quad (28a)$$

$$q_2 \approx q_1 + \frac{h}{2} L(q_1) H \omega. \quad (28b)$$

$$\approx L(q_1) q_I + L(q_1) H \left(\frac{h}{2} \omega \right) \quad (28c)$$

$$= L(q_1) \left(q_I + H \frac{h}{2} \omega \right) \quad (28d)$$

which we can use to solve for ω at the midpoint:

$$\omega = \frac{2}{h} H^T L(q_1)^T q_2 \quad (29)$$

We can now approximate the continuous-time Lagrangian using two consecutive poses, which we define as the *discrete Lagrangian*:

$$L_d(\mathbf{x}_1, \mathbf{x}_2) = h L(\mathbf{x}_{\text{mid}}(x_1, x_2), \mathbf{v}_{\text{mid}}(x_1, x_2)) \quad (30a)$$

$$= \sum_{j=1}^M \frac{1}{2} G_v(x_1^{(j)}, x_2^{(j)})^T M^{(j)} G_v(x_1^{(j)}, x_2^{(j)}) - m^{(j)} g e_3^T G_x(x_1^{(j)}, x_2^{(j)}) \quad (30b)$$

where the pose at the midpoint is approximated as:

$$Q_x(x_1, x_2) = \begin{bmatrix} \frac{1}{2}(r_1 + r_2) \\ q_1 \end{bmatrix} \quad (31)$$

and the velocity at the midpoint is approximated as:

$$Q_v(x_1, x_2) = \begin{bmatrix} \frac{1}{h}(r_2 - r_1) \\ \frac{2}{h} H^T L(q_1)^T q_2 \end{bmatrix} \quad (32)$$

To achieve higher-order integrators, simply replace these functions with higher-order quadrature rules for approximating the pose and velocity along the time step.

Using the similar techniques to those used to convert continuous-time trajectory optimization problems (17) to a discrete approximation (18), we approximate the continuous-time minimum-action problem (21) that optimizes over continuous trajectories with a discrete version that optimizes over knot points along a trajectory, evenly spaced h seconds apart:

$$\begin{aligned} & \underset{\mathbf{x}_{1:N}}{\text{minimize}} && \sum_{k=1}^{N-1} L_d(\mathbf{x}_k, \mathbf{x}_{k+1}) + \frac{h}{2} (F_k^T \mathbf{x}_k + F_{k+1}^T \mathbf{x}_{k+1}) \\ & \text{subject to} && c(\mathbf{x}_k) = 0 \end{aligned} \quad (33)$$

Here we've decided to enforce the constraints at the knot points instead of the midpoints. The pose kinematics constraint has been eliminated since we're handling it implicitly inside of our quadrature rule (32).

The first-order necessary conditions for this optimization problem are:

$$\sum_{k=1}^{N-1} \mathbb{D}_1 L_d(\mathbf{x}_k, \mathbf{x}_{k+1}) \delta \mathbf{x}_k + \mathbb{D}_2 L_d(\mathbf{x}_k, \mathbf{x}_{k+1}) \delta \mathbf{x}_{k+1} + \frac{h}{2} F_k^T \delta \mathbf{x}_k + \frac{h}{2} F_{k+1}^T \delta \mathbf{x}_{k+1} + h \lambda_k^T \mathbb{D}c(\mathbf{x}_k) = 0 \quad (34a)$$

$$c(\mathbf{x}_k) = 0, \forall k \in \mathbb{N}_N \quad (34b)$$

where $\mathbb{D}_i f(\dots)$ is the partial derivative of f with respect to the i th argument.

Re-arranging the first condition by removing the $\delta \mathbf{x}_1$ and $\delta \mathbf{x}_N$ terms from summation, we get:

$$\begin{aligned} & (\mathbb{D}_1 L_d(\mathbf{x}_1, \mathbf{x}_2) + F_1^T + h \lambda_1^T \mathbb{D}c(\mathbf{x}_1)) \delta \mathbf{x}_1 \\ & + \sum_{k=2}^{N-1} \left(\mathbb{D}_2 L_d(\mathbf{x}_{k-1}, \mathbf{x}_k) + \mathbb{D}_1 L_d(\mathbf{x}_k, \mathbf{x}_{k+1}) \right. \\ & \left. + \frac{h}{2} (F(\mathbf{x}_{k-1}, u_{k-1}) + F(\mathbf{x}_k, u_k))^T + h \lambda_k^T \mathbb{D}c(\mathbf{x}_k) \right) \delta \mathbf{x}_k \\ & + (\mathbb{D}_2 L_d(\mathbf{x}_{N-1}, \mathbf{x}_N) + F_N^T + h \lambda_N^T \mathbb{D}c(\mathbf{x}_N)) \delta \mathbf{x}_N = 0. \end{aligned} \quad (35)$$

Since $\delta \mathbf{x}_1$ and $\delta \mathbf{x}_N$ are equal to zero (no variation at the endpoints), and the summation must be equal to zero for any arbitrary $\delta \mathbf{x}_k$, then the terms of the must be equal to 0. We now obtain the *Discrete Euler-Lagrange Equation* (DEL) for a multi-body system:

$$\mathbb{D}_2^T L_d(\mathbf{x}_{k-1}, \mathbf{x}_k) + \mathbb{D}_1^T L_d(\mathbf{x}_k, \mathbf{x}_{k+1}) + \frac{h}{2} (F_{k-1} + F_k) + h \mathbb{D}c(\mathbf{x}_k)^T \lambda_k = 0. \quad (36)$$

Using (30b) and (24) we can rewrite the DEL for each individual link:

$$\begin{aligned} DEL(x_1, x_2, x_3, u_1, u_2, \lambda_2) = & DLT_2(x_1, x_2) + DLT_1(x_2, x_3) \\ & + \frac{h}{2} \left(\sum_{\bar{k}=1}^2 \sum_{i \in \mathcal{N}_1(j)} \xi_1 \left(x_k^{(j)}, x_k^{(i)}, u_k^{(j)} \right) \right. \\ & + \sum_{i \in \mathcal{N}_2(j)} \xi_2 \left(x_k^{(i)}, x_k^{(j)}, u_k^{(j)} \right) \Big) \\ & + h \left(\sum_{i \in \mathcal{N}_1(j)} \mathbb{D}_1 c \left(x_2^{(j)}, x_2^{(i)} \right)^T \lambda_2^{(ji)} \right. \\ & \left. + \sum_{i \in \mathcal{N}_2(j)} \mathbb{D}_2 c \left(x_2^{(i)}, x_2^{(j)} \right)^T \lambda_2^{(ij)} \right) = 0 \end{aligned} \quad (37)$$

where $DLT_1(x_1, x_2)$ and $DLT_2(x_1, x_2)$ are the left and right *discrete Legendre transforms*, respectively. They are derived by taking the derivative of (30b) with respect to a single pose:

$$DLT_1(x_1, x_2) = \left[\frac{-\frac{m}{h}(r_2 - r_1) - \frac{1}{2} h m g e_3}{\frac{4}{h} G(q_1)^T T R(q_2)^T H J H^T L(q_1)^T q_2} \right] \quad (38)$$

$$DLT_2(x_1, x_2) = \left[\frac{\frac{m}{h}(r_2 - r_1) - \frac{1}{2} h m g e_3}{\frac{4}{h} G(q_2)^T L(q_1) H J H^T L(q_1)^T q_2} \right] \quad (39)$$

IV. TRAJECTORY OPTIMIZATION IN MAXIMAL COORDINATES

In order to solve trajectory optimization problems in maximal coordinates, we simply replace the generic dynamics constraint in (18) with the discrete Euler-Lagrange equation and add the joint constraints. Note that since the DEL is a function of the joint forces, we need to add those as decision variables to the optimization problem.

Our new trajectory optimization problem is now of the form:

$$\begin{aligned} & \text{minimize} \quad \ell(\mathbf{x}_N) + \sum_{k=1}^{N-1} \ell(\mathbf{x}_k, u_k) \\ & x_{1:N}^{(1:M)}, u_{1:N-1}, \lambda_{2:N} \\ & \text{subject to} \quad (40) \\ & DEL(x_{k-1}^{(j)}, x_k^{(j)}, x_{k+1}^{(j)}, u_{k-1}, u_k, \lambda) = 0, \quad \forall k \in \mathbb{N}_{2,N-1}, j \in \mathbb{N}_M, \\ & c(x_k^{(i)}, x_k^{(j)}) = 0, \quad \forall k \in \mathbb{N}_N, (i, j) \in \mathcal{E} \end{aligned}$$

In order to solve (40) using Ipopt, we need to supply the constraint Jacobian with respect to all of the decision variables. Unlike standard forward simulation using variational integrators in which only derivatives with respect to x_3 are required, trajectory optimization needs the derivatives with respect to all of the inputs to the DEL equation.

V. RESULTS

An Ipopt-based solver for trajectory optimization in maximal coordinates was developed from scratch in the Julia programming language. For maximal coordinates, automatic differentiation was only used for the gradient of the cost function: the Jacobian of all constraints were derived and implemented analytically. For the minimal coordinate implementation, RigidBodyDynamics.jl was used to compute the dynamics and dynamics Jacobians (using automatic differentiation) and the dynamics were discretized using implicit midpoint integration. All timing results were obtained on an Intel i7-1165G7 processor with 16 GB of memory.

The mass and inertia properties for the double pendulum (acrobot) and robot arm were calculated assuming each link was a cylindrical body of aluminum of uniform density of 2.7 kg/m³.

A. Acrobot

The acrobot problem is a canonical benchmark problem for generating motion plans for underactuated systems. The acrobot is a double pendulum with actuation only at the “elbow” joint.

In addition to the dynamics constraints, both minimal and maximal coordinate solvers constrained the end effector to be at the upright position:

$$r_N^{(M)} + A(q_N^{(M)}) p_{ee} - r_{\text{goal}}, \quad (41)$$

where p_{ee} is the location of the end effector in the last links’s frame, and r_{goal} is the location of the goal in the world frame. For minimal coordinates, $r_N^{(M)}$ and $q_N^{(M)}$ were calculated using forward kinematics using RigidBodyDynamics.jl. The objectives for both solvers only penalized distance of the end

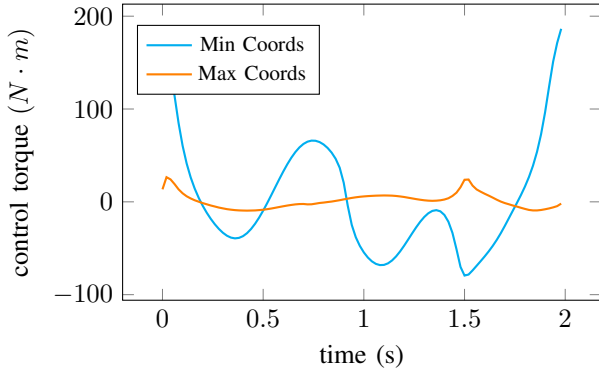


Fig. 2: Control torques for the acrobot elbow joint.

effector to the goal for all time steps, and some regularization on the control values. Both solvers were initialized with identical initial guess, which provided the initial state for all states, a control of $5t$ for the time t . The joint forces for the maximal coordinate solver were provided the forces obtained by simulating the system forward with the given control inputs. A non-zero control input and reasonable estimate of the joint forces were necessary for the solver to converge.

The joint forces from both solvers are shown in Fig. 2, and the objective and constraint violations are shown in Figs. 3 and 4. The end-effector trajectories are shown in Fig. ?? . In summary, the maximal coordinate solver found a trajectory with much lower control torques and therefore got a lower cost. As summarized in Table I, despite the fact the maximal coordinate trajectory problem is significantly larger, its cost per iteration is almost half that of minimal coordinates in this preliminary implementation. This is likely due to the fact that evaluating the dynamics Jacobian in maximal coordinates is extremely simple (not to mention extremely parallelizable) in maximal coordinates, whereas minimal coordinates require inverting the mass matrix to solve for the accelerations.

Overall, the maximal coordinate solver was much more brittle than the minimal coordinate solver. It took significantly more work to get a good trajectory in maximal coordinates. The solver had a tendency to exploit the discretization and “flip” the elbow joint in one time step, completely violating physical realistic behavior, which could only be verified by carefully analyzing the output trajectory. This behavior could be mitigated by penalizing the angular velocity of each body.

B. 6 DOF Arm

A simple 6 degree-of-freedom serial-link manipulator was modeled with similar geometry to the Kuka iiwa arm. In maximal coordinates, this model has 42 states, 6 controls, and 30 joint forces per time step. Similar to the acrobot, the arm was tasked to reach a cartesian point in the world frame. The objective minimized distance of the end effector to the goal, as well as penalizing the linear and angular velocities of each link. The midpoint velocities were calculated using the poses at adjacent times steps using the same method described in Section . Gravity was not included in this problem

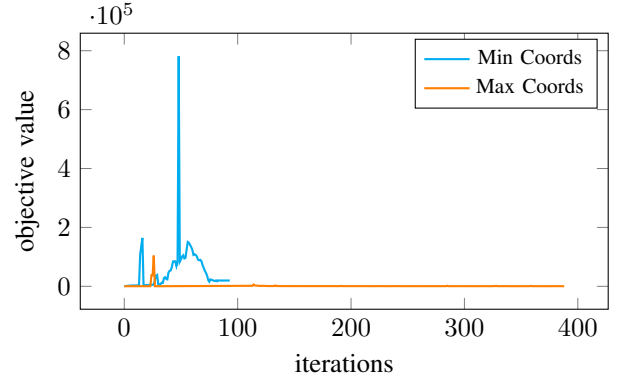


Fig. 3: Objective value for acrobot.

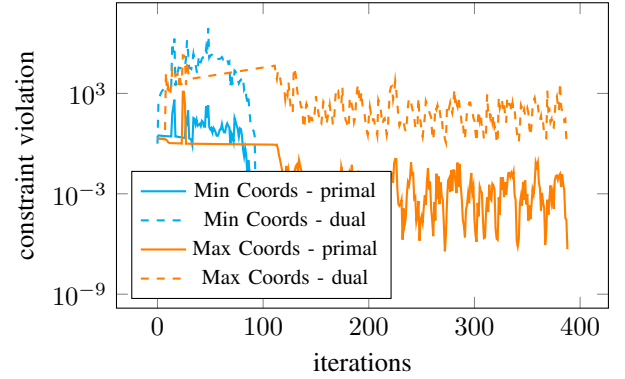


Fig. 4: Constraint violations for acrobot.

since including gravity made it extremely difficult to solve. Future work figuring out a good heuristic to do cheap gravity compensation in maximal coordinates should make it easier to find good trajectory under gravity.

A summary of the solve is given in Table . Ipopt produced a high-quality smooth trajectory (see control torques in Fig. 6). While solver converged to a high-quality trajectory, it took about 45 seconds to generate, even for a very simple a straightforward point-to-point motion task.

TABLE I: Min/Max Comparison for Acrobot

Value	Min Coords	Max Coords
Variables	504	2514
Constraints	403	2391
nnz(jac)	3606	45773
Jac density	1.8%	0.8%
Iters	93.0	388.0
Cost	19683.0	429.0
Run time (s)	6.07	11.66
Time/iter (ms)	65.0	125.0

Constraints do not include simple bounds (the initial condition), “nnz(jac)” is shorthand for the number of nonzero elements in the constraint Jacobian, and “Jac density” is the number of nonzero elements in the constraint Jacobian divided by its total size.

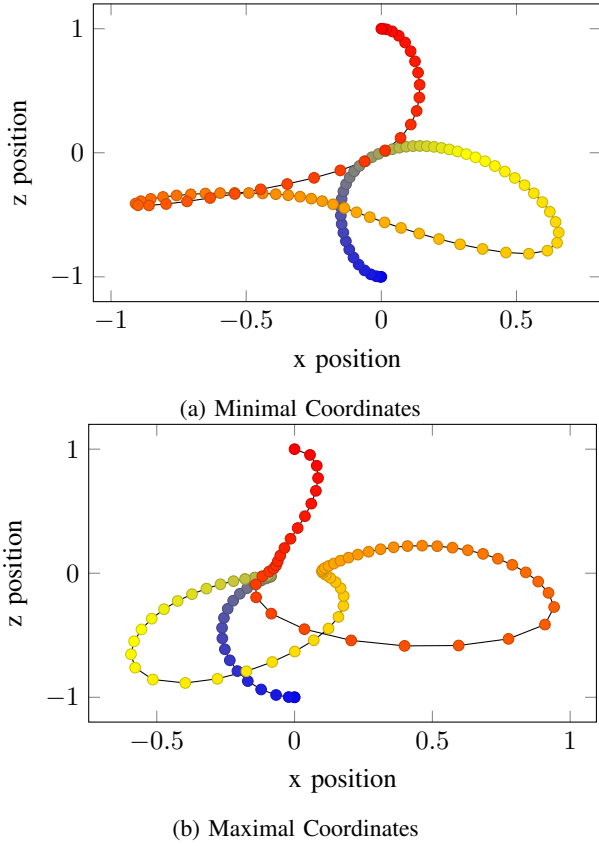


Fig. 5: End-effector location for acrobot for (a) minimal coordinates, and (b) maximal coordinates. Mark color corresponds to time, with blue being zero seconds and red being the final time.

TABLE II: Summary of Solve for 6DOF Arm

Value	6dof Arm
Variables	3942
Constraints	3567
nnz(jac)	84269
Jac density	0.6%
Iters	211.0
Cost	140.0
Run time (s)	44.21
Time/iter (ms)	210.0

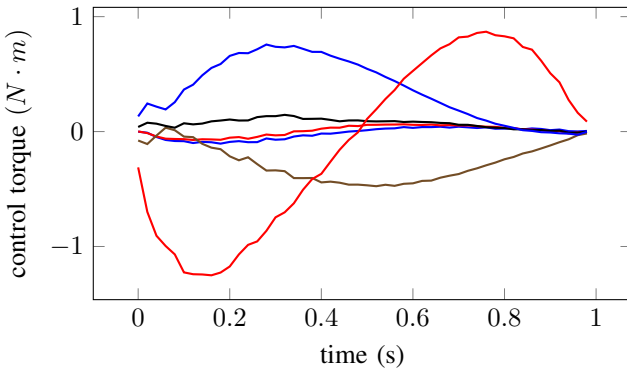


Fig. 6: Joint torques for the 6 degree-of-freedom arm.

VI. CONCLUSION

This project explored using maximal coordinates to solve trajectory optimization problems. Although maximal coordinates have some very attractive properties, using them in an off-the-shelf solver like Ipopt didn't work very well and doesn't seem to offer any sort of advantage over a minimal coordinate representation. It took significant work tuning costs and providing good initial guesses for the solver to converge. Ipopt frequently got stuck in the feasibility restoration phase and claimed infeasibility for some cost values or varying initial conditions. While the per/iteration computation time for the acrobot was surprisingly fast, it usually took many more iterations to converge than the minimal coordinate solver.

Future work could explore writing a custom solver for these types of systems. Since satisfying both the discrete Euler-Lagrange and joint constraints is relatively difficult, some sort of on- or near-manifold optimization method that takes steps that maintain dynamic and/or kinematic feasibility between solver iterations could improve convergence.

REFERENCES

- [1] S. M. LaValle, J. J. Kuffner, B. Donald, *et al.*, "Rapidly-exploring random trees: Progress and prospects," *Algorithmic and computational robotics: new directions*, vol. 5, pp. 293–308, 2001.
- [2] T. A. Howell, B. E. Jackson, and Z. Manchester, "ALTRO: A Fast Solver for Constrained Trajectory Optimization," in *IEEE/RSJ International Conference on Intelligent Robots and Systems*, Macau, China, Nov. 2019.
- [3] B. E. Jackson, T. Punnoose, D. Neamati, K. Tracy, and R. Jitosh, "ALTRO-C: A Fast Solver for Conic Model-Predictive Control," presented at the International Conference on Robotics and Automation (ICRA), Xi'an, China, 2021, p. 8.
- [4] W. Li and E. Todorov, "Iterative Linear Quadratic Regulator Design for Nonlinear Biological Movement Systems," in *ICINCO*, 2004.
- [5] C. Hargraves and S. Paris, "Direct trajectory optimization using nonlinear programming and collocation," *Journal of Guidance, Control, and Dynamics*, vol. 10, no. 4, pp. 338–342, Jul. 1, 1987.
- [6] B. E. Jackson, T. A. Howell, K. Shah, M. Schwager, and Z. Manchester, "Scalable Cooperative Transport of Cable-Suspended Loads With UAVs Using Distributed Trajectory Optimization," *IEEE Robotics and Automation Letters*, vol. 5, no. 2, pp. 3368–3374, Apr. 2020.
- [7] A. Wächter and L. T. Biegler, "On the implementation of an interior-point filter line-search algorithm for large-scale nonlinear programming," *Mathematical Programming*, vol. 106, no. 1, pp. 25–57, Mar. 2006.
- [8] P. E. Gill, W. Murray, and M. A. Saunders, "SNOPT: An SQP Algorithm for Large-Scale Constrained Optimization," *SIAM Review*, vol. 47, no. 1, pp. 99–131, Jan. 2005.

- [9] J. Brudigam and Z. Manchester, "Linear-Time Variational Integrators in Maximal Coordinates," in *Workshop on the Algorithmic Foundations of Robotics*, Oulu, Finland, Jun. 2020, p. 17.
- [10] J. Brüdigam and Z. Manchester, "Linear-quadratic optimal control in maximal coordinates," in *2021 IEEE International Conference on Robotics and Automation (ICRA)*, IEEE, 2021, pp. 9775–9781.
- [11] D. Baraff, "Linear-time dynamics using Lagrange multipliers," in *Proceedings of the 23rd Annual Conference on Computer Graphics and Interactive Techniques*, ACM, 1996, pp. 137–146.
- [12] A. Knemeyer, S. Shield, and A. Patel, "Minor change, major gains: The effect of orientation formulation on solving time for multi-body trajectory optimization," *IEEE Robotics and Automation Letters*, vol. 5, no. 4, pp. 5331–5338, 2020.
- [13] Z. Manchester and S. Kuindersma, "Variational Contact-Implicit Trajectory Optimization," in *International Symposium on Robotics Research (ISRR)*, Puerto Varas, Chile, Dec. 2017.
- [14] J. E. Marsden and M. West, "Discrete mechanics and variational integrators," *Acta Numerica*, vol. 10, pp. 357–514, 2001.
- [15] B. E. Jackson, K. Tracy, and Z. Manchester, "Planning With Attitude," *IEEE Robotics and Automation Letters*, pp. 1–1, 2021.
- [16] D. Mayne, "A Second-order Gradient Method for Determining Optimal Trajectories of Non-linear Discrete-time Systems," *International Journal of Control*, vol. 3, no. 1, pp. 85–95, Jan. 1, 1966.
- [17] Z. Xie, C. K. Liu, and K. Hauser, "Differential dynamic programming with nonlinear constraints," in *2017 IEEE International Conference on Robotics and Automation (ICRA)*, May 2017, pp. 695–702.
- [18] M. Gifftthaler, M. Neunert, M. Stäuble, J. Buchli, and M. Diehl. "A Family of Iterative Gauss-Newton Shooting Methods for Nonlinear Optimal Control." (Dec. 11, 2017), [Online]. Available: <http://arxiv.org/abs/1711.11006> (visited on 01/05/2021).
- [19] F. Farshidian, M. Neunert, A. W. Winkler, G. Rey, and J. Buchli, "An efficient optimal planning and control framework for quadrupedal locomotion," in *2017 IEEE International Conference on Robotics and Automation (ICRA)*, May 2017, pp. 93–100.